Compression of an Adsorbed Polymer Layer of Fixed Mass: A Monte Carlo Study

Jason de Joannis,[†] Jorge Jimenez,[†] Raj Rajagopalan,[†] and Ioannis Bitsanis*[,‡]

Department of Chemical Engineering, University of Florida, Gainesville, Florida 32611, and Institute of Electronic Structure & Laser, Foundation for Research and Technology—Hellas, P.O. Box 1527, Vassilka Vouton, Heraklion 711 10, Crete, Greece

Received September 15, 2000; Revised Manuscript Received March 8, 2001

ABSTRACT: Lattice Monte Carlo simulations are used to analyze the normal force induced by interacting polymer chains between an athermal plane and an adsorbing plane in an athermal (good) solvent. The simulations are carried out under conditions of "restricted equilibrium" in which the amount of polymer in the system is not allowed to fluctuate. The results are compared with numerical lattice mean-field calculations. We observe that mean-field theory usually overestimates the magnitude of the force. A substantial improvement in the comparison is obtained when interpreted with respect to properties of the corresponding unconfined layer at equilibrium with the bulk solution. For instance, in the case of high coverage, simulations and numerical mean-field theory are in good agreement at the same *relative* coverage, e.g., the same ratio of surface coverage to *saturation* coverage. Comparison with asymptotic scaling predictions does not yield unequivocal results for these chain lengths, but the results are roughly consistent with the nontrivial (−3) power law. A brief analysis of the compression of two layers against each other shows a strong similarity with the main results of this work when the surfaces bear an excess of adsorbed polymer chains (i.e., high coverage).

1. Introduction

Numerous engineering and biological processes depend crucially on the physical response of solid surfaces bearing soft polymer layers. Chemi- or physisorbed layers of polymer chains often constitute a better alternative for screening attractive van der Waals interactions than manipulation of electrostatic forces, especially in organic environments. Linking the microstructure of these layers to the mesoscopic reality of confinement will enhance our understanding and capability to control these systems. Molecular rearrangements following the compression of a physisorbed polymer layer are not fully understood. This is an important problem when dissimilar surfaces mediated by a polymer solution are in proximity, e.g., colloidal mixtures.

Several model experiments could be designed in order to study the features of single layer compression. An atomic force microscope (AFM) can be used to measure sensitively the force between a colloidal sphere and a planar surface within a liquid environment.[1] Recent experiments of this type on adsorbed polymer layers[2] have not yet addressed the case of dissimilar surfaces. A second model experiment might involve a mixture of two kinds of colloids in a polymer solution. The selection of nonadsorbing and adsorbing colloids could elicit fundamental information about compression of a single polymer layer. Toward this end, an experiment of some advantage would be the neutron diffraction of colloidal platelets bearing adsorbed polymers.[3] The primary difference, affecting the pressure, between one and two layer systems, originates from the absence of bridging in the one layer system, where bridges are replaced by long loops.

The interaction between two physisorbed layers has been the subject of extensive theoretical investigation. In 1981 and 1982, de Gennes[4] adapted the density functional approach of Cahn[5] to describe concentration gradients in polymeric systems. The result is equivalent to the *ground state* of the general self-consistent mean-field (SCMF) equation for a polymer chain (introduced by Edwards[6]), and it provides analytic access to the interaction free energy between two surfaces bearing adsorbed polymer chains in limiting cases. The mean-field approximation is inaccurate for semidilute solutions.[7] De Gennes constructed a rescaled free energy functional[4] in order to account for excluded-volume correlations neglected by the SCMF approach.

On typical relaxation and compression time scales, experimental conditions correspond to a system in restricted equilibrium.[8] "Restricted" equilibrium is restricted only in the sense that chains cannot leave or enter the gap between the two surfaces. Otherwise, chain conformations relax fully. Desorption is allowed, provided that the desorbing molecules do not leave the gap. (However, desorption is negligible under high-compression conditions.) Figure 1 is a schematic of restricted equilibrium for a system with one adsorbing surface. The number of chains within the volume enclosed by dashed lines is considered fixed. The transition from weak to strong confinement (by the upper nonadsorbing surface) is illustrated in Figure 1b,c where both the density and ratio of loop-to-tail conformations increase.

Klein, Pincus, and Ingersent[9] extended de Gennes' SCMF theory to polymer chains in Θ and poor solvents under conditions of restricted equilibrium. In another extension, Rossi and Pincus[10,11] studied the case of undersaturated polymer layers in a good solvent. The important effect of undersaturation has been documented experimentally by taking measurements during the long incubation phase of polymer adsorption.[8] Brooks and Cates[12] analyzed a more stringent case of restricted equilibrium, in which the number of surface

[†] University of Florida.
[‡] Institute of Electronic Structure & Laser.

10.1021/ma001605i CCC: $20.00
Published on Web 05/19/2001

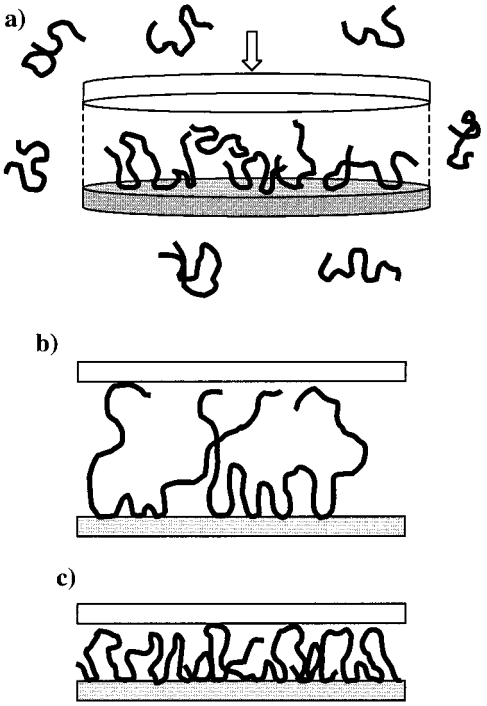

Figure 1. (a) Illustration of restricted equilibrium. The system enclosed with dashed line is closed to polymer chains (but allows solvent to drain). (b) Low-pressure system of adsorbed chains. (c) High-pressure system of adsorbed chains.

contacts (in addition to the number of polymer chains) remains constant during compression. Klein and Rossi[13] reviewed and generalized many of the theoretical results relevant to experimental observations in good solvents.

An approach that employs the first-order parameter of the SCMF Edwards equation was first used by Ji et al.[14] They complemented it with a blob-type analysis and obtained analytical results for the number and size of bridges, as well as the force of interaction. Several SCMF studies which go beyond the ground state by the use of a second-order parameter[15−18] (known to account for the effects of tails) of the SCMF Edwards equation have appeared recently. Bonet-Avalos et al.[15] obtained information on the conformations between surfaces and the concentration profile. Subsequently, Bonet-Avalos et al.[16] extended this approach to study ideal equilibrium. Semenov et al.[17] applied the same approach to restricted equilibrium, and Mendez-Alcaraz et al.[18] obtained numerical results for the same cases. These researchers reported qualitative differences in the interactions due to tail effects that are not captured at the ground-state level.

A matrix methodology for the full numerical solution of the SCMF equation which is not limited to asymptotically large chain lengths was developed by Scheutjens and Fleer.[19,20] Their approach is capable of predicting concentration profiles, conformations, and interaction energies between surfaces bearing adsorbed layers. Their lattice mean-field theory is appealing for its flexibility in examining a broad range of conditions, e.g., solvent quality, chain length, under/oversaturation, and ideal/restricted equilibrium. A numerical study[21] demonstrated the equivalence between lattice and off-lattice SCMF calculations for large chains. The lattice framework of our simulations allows for a direct comparison of our Monte Carlo (MC) data with the lattice SCMF predictions of Scheutjens and Fleer. The major limitation of the mean-field approximation originates from its inability to account properly for certain correlations, which are prevalent at semidilute concentrations.[7]

There have been few simulation studies of the forces induced by adsorbed chains, partly due to the computational difficulty of this problem. In a previous study[22] we obtained the forces between two adsorbed layers, wherein the focus was on the role of bridging forces under conditions of low polymer coverage. The present study differs in that bridging conformations are eliminated from the picture, in an effort to understand the effect of purely steric forces. A byproduct of this effort is the demonstration of similarities with the more common case of interaction between *two* surfaces bearing an excess of adsorbed polymer layers.

A similar system was studied by Pandey et al.,[23] in which chains were confined between an adsorbing and a neutral plate. An analysis of the pressure tensor was made in this system, which focused was on the surface tension of the chains at either surface when the surface-to-surface separation is large and fixed. Several studies[24,25] have addressed the kinetics and equilibrium structure of chains adsorbed from a bulk reservoir.

The surface force apparatus[26] (SFA) measures directly the forces between surfaces bearing polymer chains in a liquid environment. With use of the SFA, much progress in the measurement of forces between adsorbed polymer layers was made during the 1980s (reviewed in refs 27 and 28). All experiments were carried out in good solvent conditions, and the polymer chains were given sufficient time to adsorb fully. These studies reported monotonically repulsive forces with a range of interaction of $5-10R_g$. The largest polymer chains used in good solvent/SFA experiments were $1.2 \times 10^6 M_W$ poly(ethylene oxide) (PEO) in water.[8] These molecules were sufficiently large to test asymptotic theoretical predictions[25] provided that polydispersity ($M_W/M_N = 1.2$) did not play a substantial role. The density functional theory for good solvents mentioned above[4] yields power laws for the force profile at small and large separations. The experiments of ref 8 were consistent with the small-separation power law ($f \sim H^{-2.25}$), but a separate large-separation power law ($f \sim H^{-3}$) was difficult to discern.

Destabilization, presumably the result of bridging, is reported in SFA experiments when the surfaces are undersaturated. In a recent publication[22] we determined that substantial numbers of bridges form even under conditions of excess coverage. This simulation study reports that bridging effects are dominant under conditions of low surface coverage (undersaturation) but are overwhelmed by repulsive steric forces as the coverage increases near the saturation point.

2. Model, Monte Carlo, and Mean-Field Numerics

The model for the polymer chains is that of self-avoiding (and interavoiding) random walks (SAW's) on a simple cubic lattice, which provides a generic, coarse-grained description of polymer conformations in an athermal solvent. The space is bound in one dimension (z) and infinite in the other two dimensions (x, y). Chain segments have access to layers 1 to H. The "height" of the system, H, is a critical parameter, which, along with the temperature, chain length, N, and total number of monomers (i.e., repeat units) per unit area, Γ, defines the thermodynamic state of the system. In the simulations, as usual, the infinite width of the system is

handled with periodic boundaries, which should be larger than the longest correlation length in the system.[29] Multiple occupancy of lattice sites, as well as occupancy of sites on layers 0 and $H + 1$, is not allowed. Monomers that adsorb on the lower surface ($z = 1$) have energy $-\epsilon$ ($\epsilon > 0$), in units of the thermal energy kT.

We have previously used this model and simulation method to study the structure of interacting chains in an adsorbed layer,[25] the force induced by a single chain confined between parallel walls,[30,31] and the attractive force between two undersaturated physisorbed layers.[22] The number of steps used in each SAW (N) ranges from 50 to 1000 (bulk R_g from 4.3 to 25), which corresponds roughly to and goes well beyond the molecular weights of suspension stabilizers (for several examples see ref 25). H ranges from 3 (i.e., much smaller than R_g) to twice the bulk gyration radius. This study was made possible only through the combination of recent techniques of sampling configuration space and obtaining forces. The former of these techniques has been employed widely for the study of phase equilibria in systems with atom-based pair potentials but has seen fewer applications similar to the present one. Therefore, our description goes into some detail, so far as the method pertains to our simple lattice system.

2.1. Sampling Conformations: Configurational Bias. The configurational bias Monte Carlo method (CBMC) developed by Siepmann and Frenkel[32] is very efficient in sampling configurations of SAW's on lattices. CBMC has also been generalized to off-lattice and nonpolymeric systems.[29] A CBMC *trial* move takes place as follows: One of the chains in the system is chosen at random for modification. A "coin toss" determines which end of the chain will be the starting end. Then the chain is broken at a random position, segment γ, along its backbone. The $\gamma + 1$ to N segments are removed and regenerated using a modified Rosenbluth-biased walk[32,33] starting from the position of segment $\gamma + 1$. Each segment ($\gamma + \nu$) added during the generation of the "trial subchain" is selected to occupy one of the neighboring lattice sites of the previous segment with a certain probability. One of these sites is occupied by segment $\gamma + \nu - 1$. Thus, only the five remaining sites are considered. Associated with each of these five sites is a Boltzmann weight, $B = \exp(-\beta\varphi)$, which in this system assumes one of the following three values: φ is equal to $-\epsilon$ for unoccupied sites on the adsorption layer, 0 for all other unoccupied sites, and infinite for occupied sites. CBMC selects site i with probability

$$p_i = B_i / \sum_{j=1,5} B_j \tag{1}$$

Therefore, steps into unoccupied sites within layers 2 to H are equally likely, whereas a step into the first layer is favored by a factor of $\exp(\beta\epsilon)$.

The above prescription for generating a trial move does not satisfy detailed balance. This necessitates the introduction of a correction factor that eliminates this bias. This quantity is known as the Rosenbluth weight, W. The Rosenbluth weight is defined recursively

$$w_{i+1} = w_i / \sum_{j=1,5} B_j \tag{2}$$

where $w_1 = 1$ and the summation is again over the five possible positions of the $(i + 1)$th segment. The ratio of the A−B and B−A probabilities is equal to $\exp[-\Delta U_{AB}(W_A/W_B)]$, where ΔU_{AB} is the overall change in potential energy of the system. This leads to the following probability for accepting a trial move:

$$\min[1, W_B/W_A] \tag{3}$$

Thus, the configurational bias method for SAW's on a lattice is completely specified by definition of the elemental move (eq 1) and the acceptance rule (eqs 2 and 3). Here only the essential components of our method are presented. A thorough and more general discussion of CBMC can be found in ref 29.

2.2. Forces from Lattice Monte Carlo: Contact-Distribution Method. For the purposes of force calculation we introduce a repulsive potential, V, exerted by the upper surface ($z = H$). The Helmholtz free energy has a parametric dependence on the repulsive potential, $F_{N\Gamma HT}(V)$. The contact-distribution method[34] (CDM) supplies a procedure for calculating the change in this function caused by changes of the external potential, $\Delta F(V_1,V_2) \equiv F(V_2) - F(V_1)$. CDM minimizes the error in the calculation of the ratio of partition functions that correspond to different values of the repulsive potential V. This ratio of partition functions depends only on the number of contacts with the upper wall, n_c.

$$\frac{Q_2}{Q_1} = \sum \frac{\exp(-\beta U_2)}{\exp(-\beta U_1)} = \sum \exp[-\beta(n_{c2}V_2 - n_{c1}V_1)] \tag{4}$$

The summation is over all microstates of the system, and U refers to the potential energy of a given microstate. A general procedure has been derived for the minimization of the error in such a calculation (acceptance ratio method).[35] It requires the probability distribution for the number of contacts, $P(n_c)$, and yields the following relation:[34]

$$\sum_{n_c} \frac{P_2(n_c) - P_1(n_c)\exp(\Delta F - n_c\Delta V)}{1 + \exp(\Delta F - n_c\Delta V)} = 0 \tag{5}$$

where the subscript on P denotes either system 1 or 2 with repulsive potential V_1 or V_2. This equation is solved implicitly for the free energy.

The force, f, exerted by the polymer chains on the upper wall (or vice versa) is identified as the derivative of the Helmholtz free energy with respect to wall separation, i.e.,

$$f(H) = -\frac{\partial F}{\partial h}\Big|_H \cong \frac{F_{H-a/2} - F_{H+a/2}}{a} \tag{6}$$

Here h is used to represent the wall separation as a free variable, a is the lattice unit length, and f is the force in the direction normal to the walls, where a positive quantity expresses repulsion. The right-hand side of eq 4 is equivalent to the limit as the repulsive potential approaches infinity, i.e., $\lim_{V\to\infty}\Delta F(0,V)$. This limit can be evaluated by setting ΔV equal to infinity in eq 5, with the simple result $-(kT/a)\ln[P_{V=0}(0)]$. A sequence of simulations with incremental increases in V is required, and the zero-contact probability is eventually obtained as the limit of such incremental changes.

$$f(H) = \Delta F(0,V_1) + \Delta F(V_1,V_2) + \ldots + \Delta F(V_{t-1},V_t) - kT\ln[P_t(0)] \tag{7}$$

Thus, each term in eq 7 represents one solution of eq 5 after determining the contact probability distributions from two simulations. A total of $t + 1$ simulations are required to compute the overall change in free energy or the force. The accuracy of this approach has been subjected to several tests and is found to be quite good.[36]

Historically, the first method to obtain forces from a lattice MC simulation[37] used an ensemble average of the Rosenbluth weight but had the drawback of inefficient sampling. Dickman and co-workers[38] have proposed an alternative methodology that has been used extensively to determine equations of state for polymer solutions. This method bears certain similarities with CDM in that it employs a fictitious potential at the upper wall and requires multiple simulations per force datum. It is limited by the numerical calculation of a thermodynamic integral and by the approximations introduced in the form of the integrand.

2.3. Numerical Solution of the Lattice SCMF Equations. Several comparisons will be made with the self-consistent mean-field (SCMF) lattice theory of Scheutjens and Fleer[19] throughout this paper. The theory was extended to allow the calculation of forces for both full and restricted equilibrium.[20] The model employed by the SF theory is exactly the same as that incorporated in our MC calculations. Therefore, comparisons with MC data test directly the validity of mathematical and statistical-mechanical approximations inherent to the SCMF theory. Various refinements of this theory have been proposed, for example, the exclusion of direct backfolding of the chains.[39] However, such refinements do not alter the essence of the mean-field assumption. The two major approximations of the SF theory are the following: (i) the Bragg−Williams (i.e., random-mixing) approximation in each layer; (ii) the expression for the effective interaction between a given segment and the rest of the segments, which is based on an approximate analytical form of the equation of state for bulk polymer solutions.

Our SCMF calculations were subjected to extensive quantitative comparison with a program commercially available (PolAd). The results of the two programs on structural features were identical in all examples studied. The forces were calculated under conditions of restricted equilibrium as explained in ref 20 and were identical with the data in that publication.

3. Results

3.1. Compression of a Polymer Layer by an Athermal Wall. 3.1.1. Structural Changes upon Compression. In this section we summarize certain important changes in chain conformations that are linked to the observed variation of pressure with separation. Figure 2a−c shows the effect of compression on chain conformations. A typical chain under these conditions initially has one large tail, many large trains, and many smaller loops.

Upon compression of the outer tail dominated area, several tail segments are converted to loops and trains. The change in the latter structures is barely perceptible as the tail segments are distributed among the multitude of loops and trains. This corresponds to the broad plateaus in the loop and train data of Figure 2a,b. A closer analysis shows that in this area polymer contact with the upper surface is almost exclusively with tail segments (see Figure 2c). Over this range of interactions no free chains were observed.

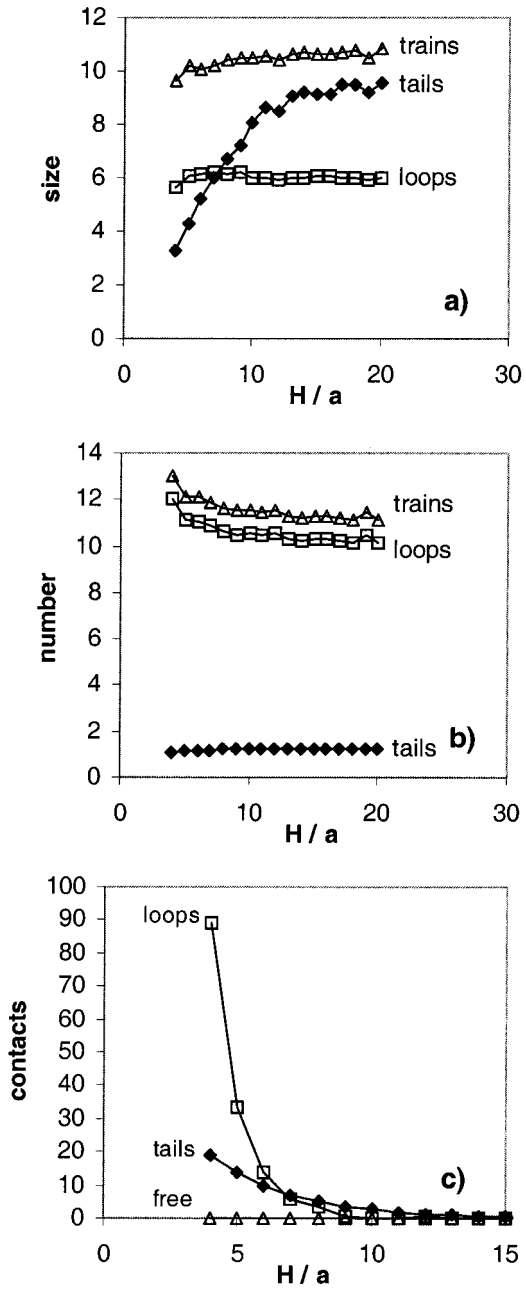

Figure 2. (a) Average size of tails, loops, and trains vs wall separation. (b) Average number of tails, loops, and trains vs wall separation. (c) Average number of contacts of tail, loop, and free-chain segments with upper wall. Parameters: $N = 200$, $\epsilon = 1.0kT$, $\Gamma = 1.0$ monolayers.

At high compressions ($H < R_g = 9.7a$) the compression of loops is evident as they multiply and become smaller, while the tails practically disappear. This is accompanied (Figure 2c) by a shift from predominant contact of the upper wall with tail segments to contact with loop segments (at $H = 7a$).

A closer analysis of the conformations is given in Figure 3, where histograms of tail, loop, and train sizes are shown at a small separation, $H = 4$. These are also compared with the results of corresponding self-consistent mean-field calculations using the Scheutjens−Fleer method.[20] Distributions generally decay monotonically with increasing size of the conformation. Quantitative differences between MC and SCMF are substantial. Of note is the effect of the cubic lattice on the number of one-segment loop and train conformations. The prob-

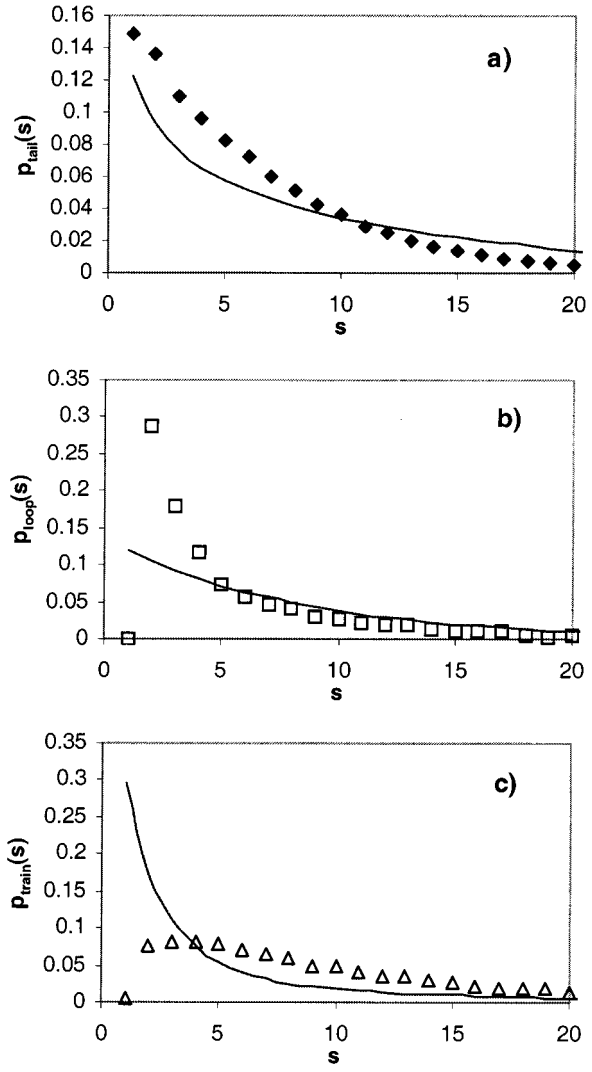

Figure 3. Comparison of MC (symbols) and SCMF (lines) for adsorbed conformation distributions. The symbol s is the number of segments in loops (a), tails (b), and trains (c). Parameters: $N = 200$, $\epsilon = 1.0\ kT$, $\Gamma = 1.0$, and $H = 4$.

ability of single-segment trains or loops is a priori zero because these can only be produced by back-folding of a chain. A diamond lattice would allow single segment trains and loops without back-folding of the chain. Although the SCMF calculations are based on a cubic lattice, back-folding is not forbidden as a consequence of the mean field in each layer. A second-order Markov SCMF method,[39] which eliminates back-folding, has been proposed, and some of these results will be presented below. A more realistic point of view is that the number of these small conformations is something between the extremes given by SCMF and MC. There may be local constraints, which lead to the depletion of short trains and loops, although not to the exaggerated extent illustrated by the simple cubic lattice model.

Further speculation as to the origins of the marked differences in the distributions is difficult. Even the tail distribution, which is the least effected by the first layer complications discussed, shows a tendency of the SCMF to generate a tail distribution that is too heavily weighted toward large tails. This discrepancy is partly the result of the lower saturation point predicted by the SCMF theory, which forces tail conformations to expand in order to avoid crowding. The consequences of these

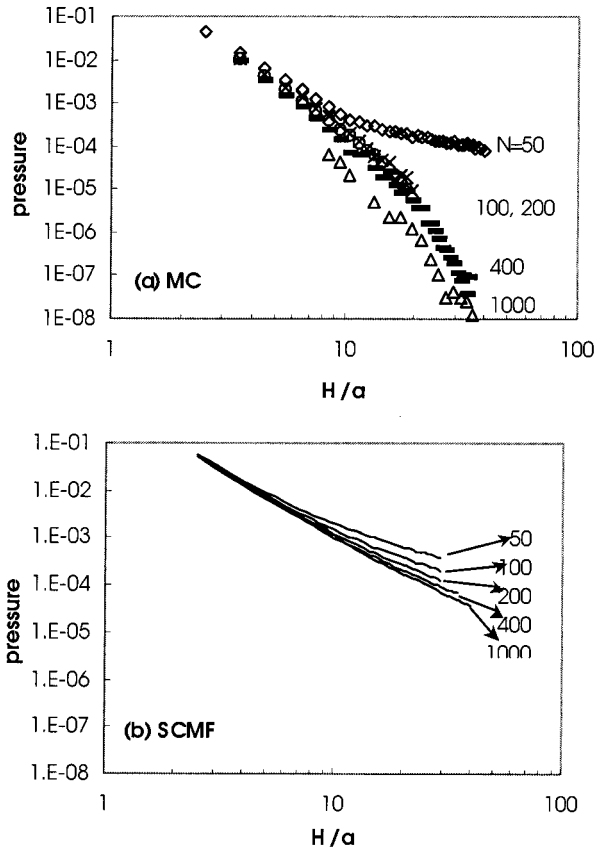

Figure 4. Pressure (units of kT/a^3) vs wall separation for MC (a) and SCMF (b) data. The adsorption energy and total coverage are $\epsilon = \chi_s = 1.0kT$ and $\Gamma = 1.0$ monolayers; chain lengths are indicated. A fit of the MC data for small separations yields approximate power laws ($p \sim H^m$) with $m = -3.3$, -3.9, -3.8, and -4.3 for $N = 50$, 100, 200, and 400, respectively.

structural differences will be discussed further in the next sections.

3.1.2. Force of Compression. In this subsection we focus on the normal force per unit area, or pressure, P_z. In Figure 4a MC data are presented for the pressure vs wall separation profile. Chain length is seen to have little quantitative effect on the pressure if the total number of polymer segments per unit area ($\Gamma = 1.0a^{-2}$) is kept constant. In particular, the curves for $N = 100$, 200, and 400 exhibit an impressive overlap. The high-pressure data appear linear on a log scale, with an exponent, m, between -3 and -4.

The fact that the $N = 50$ curve deviates from the rest and has a concave shape is explained by the saturation coverage, Γ_0, for this chain length. $\Gamma_0(N,\epsilon)$ is defined as the coverage on a surface bearing N-segment chains, with adsorption energy ϵ, at equilibrium with a bulk solution of dilute concentration (the plateau in an adsorption isotherm[25]). Adsorption isotherms are characterized by a sharp rise from zero to the saturation coverage, an almost flat (plateau) region for the dilute regime, and a gradual rise at high concentrations. Γ_0 increases slightly with chain length, and Γ_0 for $N = 200$ and $\epsilon = 1.0$ is approximately $1.2a^{-2}$. Therefore, the large chains in Figure 4a are well below their saturation point while the smallest chains ($N = 50$) are above their saturation point. The concavity of the $N = 50$ curve is due to the large number of free chains in the system. In Figure 4b the corresponding SCMF calculations show a similar independence of chain length but are otherwise

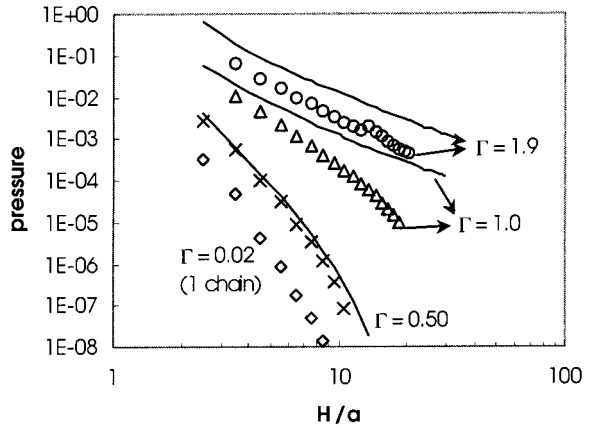

Figure 5. Pressure vs wall separation for $N = 200$ and $\epsilon = \chi_s = 1.0kT$. MC data are shown as symbols, and SCMF lattice calculations are shown as lines. The coverage (number of monolayers) is indicated on plot. A fit of the MC data for small separations yields approximate power laws ($p \sim H^m$) with $m = -2.7$, -3.8, and -5.9 for $\Gamma = 1.9$, 1.0, and 0.50 (total number of polymers segments per unit area), respectively.

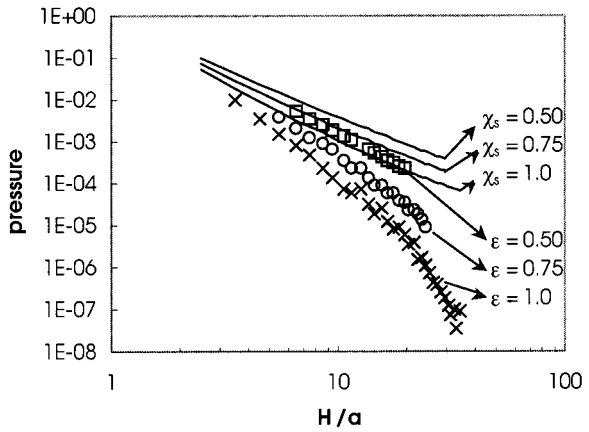

Figure 6. Pressure vs wall separation for $N = 400$ and $\Gamma = 1.0$ at three different adsorption energies. As in Figure 5, the lines represent SCMF and the symbols are MC. A fit of the MC data for small separations yields approximate power laws ($p \sim H^m$) with $m = -2.9$, -3.8, and -4.3 for $\epsilon = 0.50$, 0.75, and 1.0, respectively.

qualitatively and quantitatively different. Except at the smallest separations shown, the SCMF pressure is several orders of magnitude higher than MC. Also, the SCMF curves seem to have a concave shape akin to that of the $N = 50$ MC curve.

Figure 5 gives the pressure profile for three different surface coverages as well as for a single chain simulation. As anticipated, an undersaturated layer produces a sharper pressure profile with a smaller range of interactions. The exponent exhibited by the $\Gamma = 1.9$ curve, -2.7, is close to the nontrivial value predicted by de Gennes (-3) for the two-layer problem under saturated, semidilute conditions.[5] The bulk concentration that corresponds to this saturation coverage is 0.1. De Joannis et al.[25] observed a closer agreement on several configurational features of physisorbed layers with scaling predictions for moderate chain lengths, when the bulk solution is more concentrated. SCMF curves again exhibit higher pressures.

The forces at large separations in Figures 4 and 5 are generally consistent with recent experiments, which reported exponential decay in the long-range forces between two adsorbed layers.[40] Although the conditions were different (i.e., liquid−liquid and air−liquid interface), an exponential decay in the periphery of the force profile is supported by the theoretical structure of the tails in this region.[17] The $N = 200$ data in Figure 4 are probably the closest to experimental conditions in which adsorption took place from a dilute solution, since this system is close to the saturation coverage. This series crosses over from a power law to exponential decay at a distance roughly equal to the bulk radius of gyration ($9.8a$). This change is probably correlated with the shift toward long tails, as shown in Figure 2a,c. The range of forces depicted in Figures 4 and 5 is estimated as 10^4-10^{-1} N/m^2 ($10^{-2}-10^{-7}kT/a^3$). Therefore, we are probing a wide range of forces, which covers both the short-range forces measured by SFA experiments[13] and the weaker exponentially decaying forces.

The physics of compression of a two-layer system under these conditions have much in common with the one-layer system of the present study. Under high compression a dense "upper" adsorbed layer is almost impermeable to chains emanating from the "lower" surface. Therefore, in a good solvent, the "upper" layer acts as a "rough nonadsorbing surface". The scale of "roughness" should be segmental for $N = 200$ and the polymer concentrations of Figure 5.[22] Although bridging is present even in high-coverage two-layer systems, bridging forces constitute a minute component of the overall force, which is dominated by steric repulsion under these conditions.

As a limiting case, one simulation was carried out using a single 200-segment chain on a 100×100 surface. These results, plotted in Figure 5 (diamond symbols), illustrate the limiting behavior of the pressure profile for ultralow coverages when the chains no longer overlap on the surface. A physically meaningful parameter to characterize the crossover from a moderately undersaturated to a starved (no chain overlap) surface could be called the overlap coverage, Γ^*, in analogy to the overlap concentration of a bulk polymer solution. The lateral component of the radius of gyration of a single 200-segment adsorbed chain is $31a$, and the rms thickness is $1.2a$ (for large H). Visualizing the chain as a thin disk then, the overlap coverage is $\Gamma^* \approx 2N/\pi R_{gx}^2 = 0.13$ (seg/a^2). The factor of 2 is introduced to account for the fact that approximately half the segments lie on the first and the other half on the second layer.

Next, the effect of adsorption strength is analyzed in Figure 6. The compactness of strongly adsorbed layers yields sharper profiles. The comparison with the predictions of SCMF theory involved the identification of the Scheutjens−Fleer χ_s with the MC ϵ.

3.1.3. Comparison with Mean-Field Calculations: Corresponding States Principle. In this subsection we test the intuitively appealing renormalization $P(H/t,\Gamma/\Gamma_0)$. Here t is some measure of the original "layer thickness" before the onset of compression, and Γ_0 is the saturation coverage defined earlier. This analysis is similar to the principle of corresponding states of classical thermodynamics. However, it should be noted that there is as yet no fundamental basis for it. As suggested by one of the reviewers, a "blob-type" analysis could justify such a renormalization when both the unperturbed and confined layers are semidilute or concentrated.

Figures 7−10 examine whether a corresponding-states analysis applies to this system. SCMF results with a lower coverage than those in Figure 4b are presented in Figure 7. This produces a better qualitative

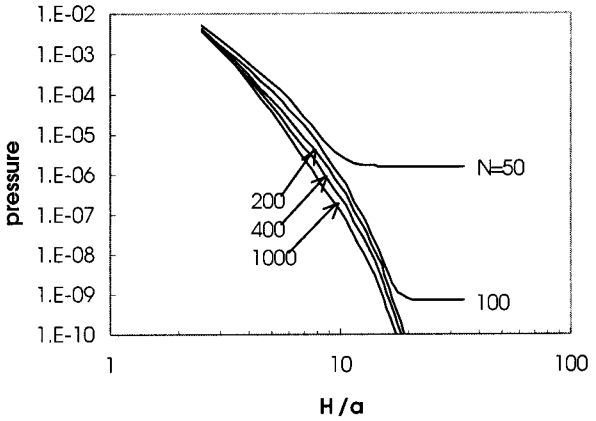

Figure 7. SCMF pressure vs separation profiles. Same conditions as Figure 4b except a lower adsorbed amount, $\Gamma = 0.50$ (monolayers), is used which produces approximately the same "reduced" coverages, $\Gamma_r = \Gamma/\Gamma_0$, as the MC systems of Figure 4a.

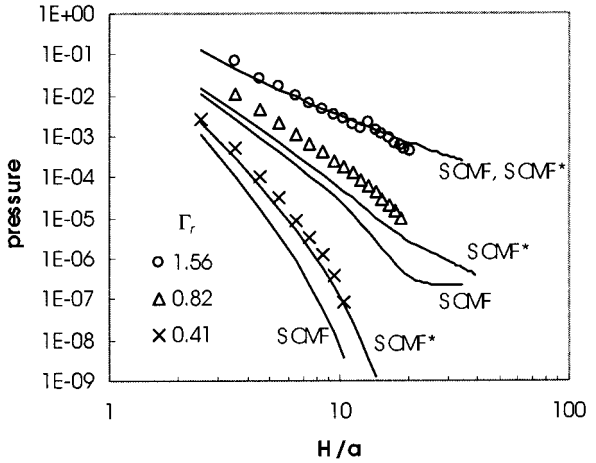

Figure 8. Same MC data as Figure 5 compared against SCMF and SCMF* (chain back-folding not allowed) of the *same reduced* coverages: $\Gamma_r = \Gamma/\Gamma_0 = 1.56$, 0.82, and 0.41.

correspondence with the simulation results of Figure 4a because the reduced coverages are closer (due to the fact that SCMF in general has a smaller Γ_0). Note that, as with the MC data in Figure 4a, only the $N = 50$ curve has a strongly concave shape. In Figure 8, the $N = 200$ simulation data are compared with SCMF calculations for the same reduced coverage. As anticipated, the best agreement for the power law and magnitude of forces is obtained for an "over"saturated surface ($\Gamma_r = 1.56$). Substantial improvement on the SCMF results for low reduced coverages is observed when the statistics include only non-back-folding conformations.[39] This is evidence that *intrachain interactions* play the most important role in shaping the properties of *starved* systems. Yet, a marked discrepancy continues to exist for the intermediate coverages ($\Gamma_r = 0.82$), where *semidilute* conditions prevail, *even when non-back-folding conformations are considered*.

Data for a number of different chain lengths, coverages, and adsorption strengths are plotted in Figure 9. Clearly, the relative sharpness (or steepness) of a profile is primarily a function of reduced coverage Γ_r. Specifically, the top two curves in Figure 9 (circles and crosses) almost overlap, despite the different chain lengths (200 and 400) and adsorption energies ($1.0kT$ and $0.5kT$). However, these two systems are characterized by almost identical Γ_r's (1.56 and 1.41). Similar comments apply

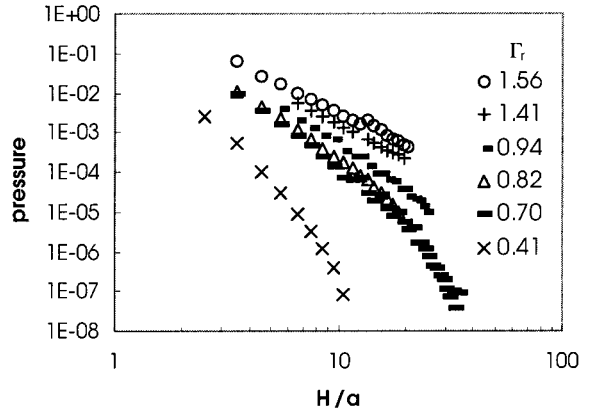

Figure 9. MC data from Figures 5 and 6 presented together and interpreted in terms of their reduced coverages, Γ_r. Starting from the largest Γ_r these are as follows: (1-circles) $N = 200$, $\epsilon = 1.0$, $\Gamma = 1.9$, $\Gamma_0 = 1.2$; (2-plus symbols) $N = 400$, $\epsilon = 0.5$, $\Gamma = 1.0$, $\Gamma_0 = 0.71$; (3-small dashes) $N = 400$, $\epsilon = 0.75$, $\Gamma = 1.0$, $\Gamma_0 = 1.1$; (4-triangles) $N = 200$, $\epsilon = 1.0$, $\Gamma = 1.0$, $\Gamma_0 = 1.2$; (5-large dashes) $N = 400$, $\epsilon = 1.0$, $\Gamma = 1.0$, $\Gamma_0 = 1.4$; (6-crosses) $N = 200$, $\epsilon = 1.0$, $\Gamma = 0.5$, $\Gamma_0 = 1.2$.

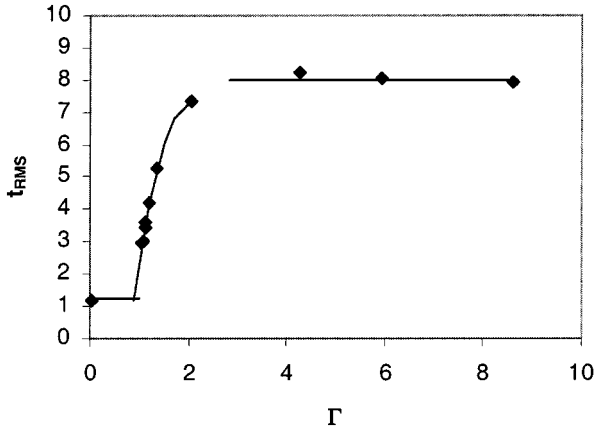

Figure 10. Rms layer thickness vs adsorbed amount for a polymer layer at equilibrium with a bulk solution of various concentrations. Data taken from ref 25; $N = 200$ and $\epsilon = 1.0kT$.

to the group of the next three curves in Figure 9. The marked discrepancy of the lowest curve from the group can be attributed to severe undersaturation quantified by the low Γ_r.

A further normalization involving the second natural variable introduced earlier, namely the unperturbed root-mean-square layer thickness (t_{rms}), will be attempted below. Independent determination of t_{rms} is difficult. First, t_{rms} is concentration-dependent, as illustrated in Figure 10. (The data are from ref 25, where the known qualitative features of this quantity were reproduced by MC simulations for which $N = 200$, $\epsilon = 1.0$, and $\Gamma_0 = 1.2$.) The thickness t_{rms} exhibits a plateau over a wide range of concentrations in the dilute regime. The existence of this plateau allows an approximate determination of t_{rms}, when the surface is "saturated" (i.e., when the bulk concentration exceeds the threshold value beyond which the plateau forms). MC simulations can also determine t_{rms} over a limited range of ultradilute bulk densities that lead to undersaturation of the surface (Figure 10). However, MC simulations cannot produce the full curve for t_{rms} at ultralow surface coverage. Our best attempt for an independent MC "measurement" of t_{rms} inside the lower portion of the ultradilute regime is represented by the first point in Figure 10, which was determined from the *single chain*

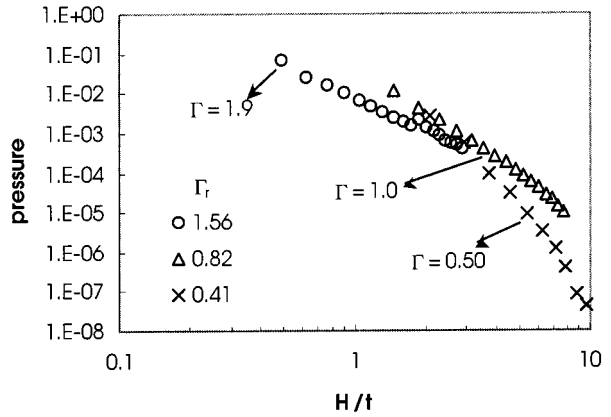

Figure 11. MC data for $N = 200$ where x-axis is normalized by the approximate RMS layer "thickness"; $t_{rms} = 1.2$, 2.4, and 7.2a for $\Gamma = 0.50$, 1.0, and 1.9, respectively.

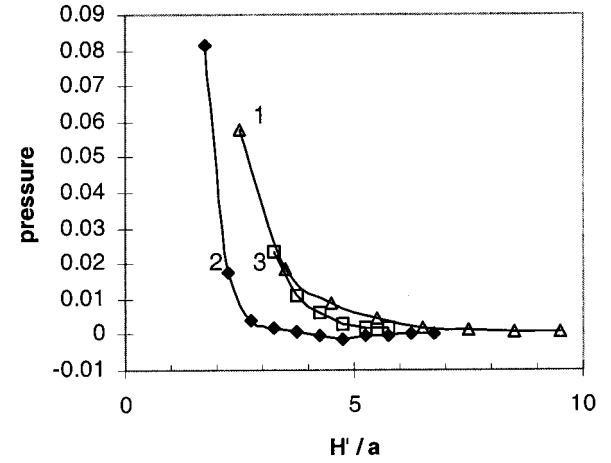

Figure 12. MC simulations for (1) one polymer layer compressed by athermal wall with coverage $\Gamma = 1.125$, (2) two polymer layers with $\Gamma = 2.25$—abscissa values represent separation between one surface and midplane; (3) two polymer layers with no bridging.

simulation discussed earlier. On the basis of this approach, the t_{rms} values that correspond to the coverages in the force simulations ($\Gamma = 0.50$, 1.0, and 1.9) were 1.2, 2.4, and 7.2, respectively.

The outcome of this second scaling, with t_{rms} as the length unit, is depicted in Figure 11. We observe a fair collapse of the data in Figure 9 (symbols are the same) over a wide range of *reduced* surface coverages (from 0.41 to 1.56). Clearly, the proposed double scaling is not perfect. However, it appears to capture the bulk of the force vs distance quantitative dependence. It can be a useful empirical tool and hopefully an inspiration for deeper theoretical understanding.

3.2. Interaction between Two Polymer Layers. Some quantification is desired concerning the differences between one- and two-layer systems, as discussed in the Introduction. For this purpose the results of three simulations will be presented: (1) a one-layer simulation, (2) a two-layer simulation, and (3) a two-layer system with no bridging. The data for the second system were taken from ref 22. The third simulation involved modified wall−segment potentials. Specifically, chains were tagged in a way that made half of them attracted to the lower wall only, while the other half experienced a similar attraction to the upper wall. The two-layer simulations were carried out using twice the number of polymer chains as in the one-layer system.

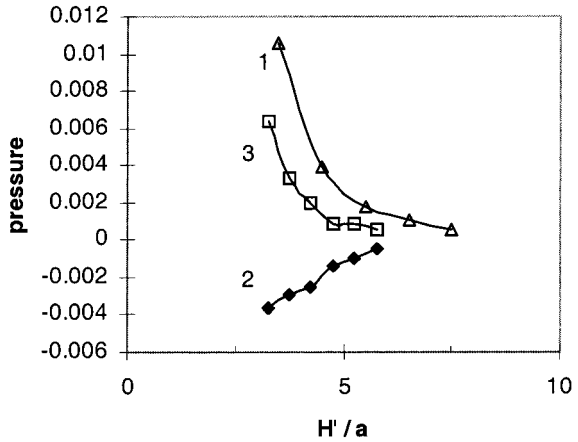

Figure 13. MC simulations for (1) one polymer layer compressed by athermal wall with coverage $\Gamma = 1.0$, (2) two polymer layers with $\Gamma = 2.0$—abscissa values represent separation between one surface and midplane; (3) two polymer layers with no bridging.

Since the coverage in Figure 12 is near the saturation point, bridging is prevalent, as it lowers the pressure by 2−3 orders of magnitude. The pressure in the one-layer system is in very good agreement with the nonbridging two-layer system. On the basis of the data for other coverages in two layer systems of ref 22, the role of bridges is dominant below $\Gamma = 2.25$ and diminishes substantially above this coverage. (Simulations above this coverage are difficult.) Therefore, we would expect the pressure profiles in one- and two-layer systems to be quite close for larger coverages.

An example of an undersaturated system is shown in Figure 13. Here a strong attraction arises in the two-layer system as a consequence of bridging without much steric competition. In this case there is a larger difference between the no-bridging curve and the one-layer curve. This may be the consequence of low polymer concentration, which allows substantial layer interpenetration.

4. Discussion and Summary

We have carried out lattice Monte Carlo simulations for the compression of an adsorbed layer of homopolymers under conditions of restricted equilibrium. The energetic response of physisorbed layers to local or macroscopic probes is of continuing experimental interest and will ultimately provide a deeper understanding of engineering processing of colloidal systems.

Furthermore, we have presented several comparisons with the numerical predictions of the lattice-mean-field theory of Scheutjens and Fleer.[19,20] Besides its broad usage, the SF approach is not limited by long chain length requirements. A direct comparison of MC data with SF predictions is disappointing (Figures 3 and 4). Much better agreement is observed when SF and MC are compared under the *same reduced coverage* (e.g., surface saturation; Figure 8).

For the same reduced coverage, good agreement is found for dense films where, as expected, the mean-field premises are justified (Figure 8). On the other extreme (e.g., starved layers and dilute films), agreement between SF and MC improves considerably when the non-back-folding version of SF is employed.[39] This stresses the importance of intrachain *and local* interactions under *dilute* conditions. When the layer can be classified as semidilute, none of the above remedies suffices

(Figure 8). The non-back-folding conformations[39] approach remains distant from the MC data. This persistent discrepancy illustrates the limitations of mean-field theories.

It has been argued that an appropriate comparison between MC and SF data should involve the same ϕ/ϕ^*, where ϕ^* is the overlap concentration in the bulk. This implies that ϕ^* is different for SF and MC. We are not aware of any reports to this effect. On the contrary, the prototype of a SCMF theory for a single chain[6] correctly predicts the Flory exponent (i.e., the chain size under good solvent conditions) and hence ϕ^*. A thorough address of this matter would involve a detailed analysis of the self-consistency issue and its implementation by specific theories. This is clearly beyond the scope of the current paper. On a more technical level, the selection of a characteristic density ϕ, in reference to an external standard, i.e., a bulk solution, is by definition impossible under conditions of *restricted equilibrium*.

The main findings of this work can be summarized as follows:

(1) Tail conformations make first contact with the compression surface. Loops and trains multiply and diminish in size with stronger compression, as tails virtually disappear at a separation of approximately $1R_g$. This provides a "visualization" of the microscopic interactions present in experiments.

(2) Differences appear in the conformation distribution between MC and SCMF and more importantly in the force profiles. The SCMF theory substantially overestimates the polymer-induced force. This is partly a consequence of the fact that the layer becomes saturated at a lower coverage for SCMF calculations than for MC calculations. When comparison is across the same reduced coverages, the thinner SCMF layer naturally leads to lower pressures than MC.

(3) The normal component of the force (sometimes referred to as pressure) depends on separation, adsorption energy, chain length, and total amount of polymer between the plates. A reduction in number of degrees of freedom from 4 to 2 is achieved when the results are scaled using characteristic properties of unperturbed layers.[25] This scaling produces a satisfactory collapse of data from several simulations under different conditions (chain length, adsorption energy, surface coverage) and generally improves the agreement of SCMF results with MC.

(4) The compression of a single layer is very similar to the compression of two physisorbed against each other, when the surfaces are saturated, or oversaturated (i.e., polymer concentration semidilute, or higher). This point was illustrated by carrying out simulations in which bridges were disallowed.

Acknowledgment. The authors acknowledge partial financial support from the US National Science Foundation through the Engineering Research Center (ERC) for Particle Science and Technology at the University of Florida (Grant EEC-9402989). The authors thank Professor S. Obukhov for many useful discussions and the reviewers for their constructive comments and suggestions.

References and Notes

(1) Ducker, W. A.; Senden, T. J.; Pashley, R. M. *Nature* **1991**, *353*, 239.
(2) Biggs, S. *Langmuir* **1995**, *11*, 156. Braithwaite, G. J. C.; Howe, A.; Luckham, P. F. *Langmuir* **1996**, *12*, 4224. Braithwaite, G. J. C.; Luckham, P. F. *J. Chem. Soc., Faraday Trans.* **1997**, *93*, 1409. Giesbers, M.; Kleijn, J. M.; Fleer, G. J.; Cohen Stuart, M. A. *Colloids Surf. A* **1998**, *142*, 343.
(3) Swenson, J.; Smalley, M. V.; Hatharasinghe, H. L. M. *Phys. Rev. Lett.* **1998**, *26*, 5840.
(4) de Gennes, P.-G. *Macromolecules* **1981**, *14*, 1637; **1982**, *15*, 492.
(5) Cahn, J. *J. Chem. Phys.* **1977**, *66*, 3667.
(6) Edwards, S. F. *Proc. Phys. Soc.* **1965**, *85*, 613.
(7) des Cloiseaux, J.; Jannink, G. *Polymers in Solution: Their Modelling and Structure*; Oxford Science Publications: Clarendon Press: Oxford, 1990.
(8) Luckham, P. F.; Klein, J. *J. Chem. Soc., Faraday Trans.* **1990**, *86*, 1363.
(9) Klein, J.; Pincus, P. *Macromolecules* **1982**, *15*, 1129. Ingersent, K.; Klein, J.; Pincus, P. *Macromolecules* **1986**, *19*, 1374; **1990**, *23*, 548.
(10) Rossi, G.; Pincus, P. *Europhys. Lett.* **1988**, *5*, 641.
(11) Rossi, G.; Pincus, P. *Macromolecules* **1989**, *22*, 276.
(12) Brooks, J. T.; Cates, M. E. *Macromolecules* **1992**, *25*, 391.
(13) Klein, J.; Rossi, G. *Macromolecules* **1998**, *31*, 1979.
(14) Ji, H.; Hone, D.; Pincus, P.; Rossi, G. *Macromolecules* **1990**, *23*, 698.
(15) Bonet-Avalos, J.; Johner, A.; Joanny, J.-F. *J. Chem. Phys.* **1994**, *101*, 9181.
(16) Bonet-Avalos, J.; Joanny, J.-F.; Johner, A.; Semenov, A. N. *Europhys. Lett.* **1996**, *35*, 97.
(17) Semenov, A. N.; Joanny, J.-F.; Johner, A.; Bonet-Avalos, J. *Macromolecules* **1997**, *30*, 1479.
(18) Mendez-Alcaraz, J. M.; Johner, A.; Joanny, J.-F. *Macromolecules* **1998**, *31*, 8297.
(19) Scheutjens, J. M. H. M.; Fleer, G. J. *J. Phys. Chem.* **1979**, *83*, 1619; **1980**, *84*, 178.
(20) Scheutjens, J.; Fleer, G. J. *Macromolecules* **1985**, *18*, 1882.
(21) Johner, A.; Bonet-Avalos, J.; van der Linden, C.; Semenov, A.; Joanny, J. *Macromolecules* **1996**, *29*, 3629.
(22) Jimenez, J.; de Joannis, J.; Bitsanis, I.; Rajagopalan, R. *Macromolecules* **2000**, *33*, 8512.
(23) Pandey, R. B.; Milchev, A.; Binder, K. *Macromolecules* **1997**, *30*, 1194.
(24) Zajac, R.; Chakrabarti, A. *J. Chem. Phys.* **1996**, *104*, 2418. Lin, Z.-Z.; Wang, W.; Ebner, C.; Nikas, Y. *Phys. Rev. E* **1993**, *48*, 1246. Lai, P.-Y. *Macromolecules* **1995**, *28*, 5742. King, S. M.; Cosgrove, T. *Macromolecules* **1993**, *26*, 5414. Wang, Y.; Rajagopalan, R.; Mattice, W. L. *Phys. Rev. Lett.* **1995**, *74*, 2503.
(25) de Joannis, J.; Thomatos, J.; Park, C.; Bitsanis, I. *Langmuir* **2001**, *17*, 69.
(26) Israelachvili, J. N.; Adams, G. E. *J. Chem. Soc., Faraday Trans. 1* **1978**, *74*, 975.
(27) Luckham, P. F. *Adv. Colloid Interface Sci.* **1991**, *34*, 191.
(28) Patel, S. S.; Tirrell, M. *Annu. Rev. Phys. Chem.* **1989**, *40*, 597.
(29) Frenkel, D.; Smit, B. *Understanding Molecular Simulation*; Academic Press: San Diego, 1996.
(30) de Joannis, J.; Jimenez, J.; Rajagopalan, R.; Bitsanis, I. *Europhys. Lett.* **2000**, *51*, 41.
(31) Jimenez, J.; de Joannis, J.; Bitsanis, I.; Rajagopalan, R. *Macromolecules* **2000**, *33*, 7157.
(32) Siepmann, J. I.; Frenkel, D. *Mol. Phys.* **1992**, *75*, 59.
(33) Rosenbluth, M. N.; Rosenbluth, A. W. *J. Chem. Phys.* **1955**, *23*, 356.
(34) Jimenez, J.; Rajagopalan, R. *Eur. Phys. J. B* **1998**, *5*, 237.
(35) Bennet, C. *J. Comput. Phys.* **1976**, *22*, 245.
(36) Jimenez, J. Ph.D. Thesis, University of Florida, Gainesville, FL, 2000.
(37) Ishinabe, T. *J. Chem. Phys.* **1985**, *83*, 423.
(38) Dickman, R.; Hong, D. *J. Chem. Phys.* **1991**, *95*, 4650. Dickman, R.; Anderson, P. E. *J. Chem. Phys.* **1993**, *99*, 3112.
(39) Leermakers, F. A. M.; Scheutjens, J. M. H. M.; Gaylord, R. J. *Polymer* **1984**, *25*, 1577.
(40) Mondain-Monval, O.; Espert, A.; Omarjee, P.; Bibette, J.; Leal-Calderon, F.; Philip, J.; Joanny, J.-F. *Phys. Rev. Lett.* **1998**, *80*, 1778.

MA001605I